

## Two-tier symmetry-breaking model of patterns on a catalytic surface

L. M. Pismen,<sup>1,2</sup> R. Imbühl,<sup>3</sup> B. Y. Rubinstein,<sup>1</sup> and M. I. Monin<sup>1</sup>

<sup>1</sup>Department of Chemical Engineering, Technion, Technion City, 32000 Haifa, Israel

<sup>2</sup>Minerva Center for Nonlinear Physics of Complex Systems, Technion, Technion City, 32000 Haifa, Israel

<sup>3</sup>Institut für Physikalische Chemie und Elektrochemie, Universität Hannover, D-30167 Hannover, Germany

(Received 19 August 1997; revised manuscript received 6 April 1998)

We present a two-tier symmetry-breaking model on a catalytic surface mediated by propagating transition fronts on two different scales. On the microscopic (nanoscale) level, there is a competition between two alternative surface phases biased by the local level of a diffusing species. On the microscopic scale, relative abundance of surface phases acts as a refractive variable biasing the balance between alternative states of the diffusive activator, thereby causing either global oscillations or domain oscillations and spiral waves in an extended system. The distribution of surface phases evolves on a longer time scale due to a curvature effect, exhibiting a kind of a ripening process coupled with oscillatory dynamics. [S1063-651X(98)13506-7]

PACS number(s): 82.65.Jv, 05.70.Ln

### I. INTRODUCTION

Single-crystal studies of catalytic CO oxidation on Pt surfaces conducted in recent years revealed a whole range of different spatiotemporal patterns [1–6]. On Pt(110), besides elementary patterns like spiral waves [1,3], complex structures involving different types of patterns on different length scales were also found [6]. The mechanism of the rate oscillations and patterns is based on adsorbate-induced surface phase transitions that are controlled by critical adsorbate coverages, i.e., the  $1 \times 1 \rightleftharpoons 1 \times 2$  transition in the case of Pt(110) and the  $1 \times 1 \rightleftharpoons$  hexagonal phase transition in the case of Pt(100) [1,2,7,8]. The phase transition affects the reaction rate through the variation of the oxygen sticking coefficient which for Pt(100) is 2–3 orders of magnitude higher on the  $1 \times 1$  surface than on the reconstructed phase, whereas the corresponding factor for Pt(110) is only about 1.5.

At this time, the standard kinetic model of CO oxidation on Pt(110) includes three dynamic variables, the CO and oxygen coverage, and the fraction of the surface occupied by one of the alternate phases (surface variable) [9]. The equations for the adsorbate coverages contain the usual kinetic expressions of the Langmuir-Hinshelwood type where the coefficients can be made dependent on the surface variable, thus accounting for the different adsorption rates and binding energies on the two surface phases; actually, the decisive difference turned out to be the difference in the oxygen sticking coefficient. The phenomenological dynamic equation for the surface variable is constructed in such a way that the less active  $1 \times 2$  phase is present at low CO coverage and the more active  $1 \times 1$  phase exists at high CO coverage.

Although the model contains three dynamic variables, it turned out to be qualitatively equivalent to a two-variable model, and can be mapped on a standard FitzHugh-Nagumo (FN) system [10]. The oxygen coverage is more or less slaved to the CO coverage which plays the role of a “fast activator.” At a fixed surface phase composition, two alternate stationary states may be attained: one with a high CO coverage that blocks the oxygen access and thereby stifles the reaction, and another with a low CO coverage and higher

reaction rate. This bistability phenomenon is common for bimolecular reactions with Langmuir-Hinshelwood kinetics. The domains with prevailing alternative stationary states evolve dynamically due to a relatively slow surface phase transition, so that the surface variable plays the role of a “slow inhibitor.”

The surface phase transition acts in such a way that the fraction of the  $1 \times 1$  phase increases on a surface patch with a high CO coverage, leading to an increased O<sub>2</sub> adsorption rate and eventually to a transition to the alternate state, and *vice versa*. In a lumped system, this leads to relaxation oscillations, and in a spatially extended system, to propagation of surface activity waves, forming either spiral waves, target patterns, or isolated mobile wave fragments [1,9–12]. The geometry of the emerging spatiotemporal structures is strongly affected by the anisotropy of surface diffusivities—a property that distinguishes patterns on surfaces from chemical patterns in liquid phase reactions. Global interactions through the gas phase serve as an additional source of dynamic complexity leading to standing waves and cellular structures [3–6,10,13,14].

The model by Krischer, Eiswirth, and Ertl [9] yields a realistic (at least in the qualitative sense) picture of kinetic oscillations and pattern formation on the Pt(110) surface. Its disadvantage, however, is that it does not lend itself to a formal treatment of the dynamics of surface reconstruction, described in a purely phenomenological way with the help of a piecewisely defined function of the CO coverage that insures correct behavior fitting the experimental data. The model also fails to take into account slow changes in catalytic activity which may be caused by surface roughening and faceting [15–17]. These two aspects are in fact related, since surface roughening is likely to occur as a result of repeated transitions between the two surface phases, which, due to their different density of surface atoms, involve a mass transport of Pt atoms [18]. Roughening or faceting might be incorporated into the kinetic model in a natural way if the phase transition could be described more realistically by means of a microscopic model.

In this paper, we present a two-tier symmetry-breaking model treating the surface phase transition explicitly and re-

placing the phenomenological equation of the surface variable by a microscale model that would describe dynamics of domains corresponding to the two surface phases. The essence of the model is the assumption that the surface phase transition is a slow local process that leads to the formation of a nanoscale pattern of surface phases, and manifests itself in slow motion of interphase boundaries with the speed being dependent on the local value of CO coverage. In turn, the visible (microscale) coverage pattern is determined by average abundance of surface phases within the diffusional range of the adsorbed species. The faceting of the surface may be directly correlated in this model with the motion of interphase boundaries, and takes place each time a certain location is passed by the phase transition front.

## II. COARSE-GRAINED TWO-TIER MODEL

Our current aim is to sketch a skeleton model that can be treated semianalytically to construct a qualitatively faithful dynamic description. We shall operate, therefore, with the simplest possible nonlinear elements suitable for our purpose and neglect such realistic details as anisotropic diffusion. Rather than considering realistic kinetic equations for the adsorbate coverages, we shall use a single equation for concentration of a fast activator  $v$  that can relax to any of two alternate states. The simplest suitable evolution equation of  $v$  is

$$v_t = \nabla^2 v + (1 - v^2)v - \eta. \quad (1)$$

As in the standard FN model, the two states are biased by the level of the inhibiting variable  $\eta$ , which is defined here in such a way that the level  $\eta = 0$  corresponds to the Maxwell construction of the two alternate macrostates. We interpret it here as a surface state variable that models the inhibiting action of the  $1 \times 2$  reconstruction. In view of the long diffusional range of CO adsorbate (modeled by the activator concentration  $v$ ), the variable  $\eta$  should be *coarse grained*. We shall interpret it as the *local average* fraction of one of the surface phases computed by spatial averaging over a surface area within the diffusional range of  $v$ . The activator acts as a pattern-forming agent on a large scale corresponding to the diffusional range of a mobile adsorbed species (CO). This is the visible pattern observed experimentally on a  $10^{-4} - 10^{-2}$  cm scale. The surface variable  $\eta$ , which is slow and nondiffusive, plays the same role of a refractory variable as in the model by Krischer, Eiswirth, and Ertl [9].

The distinctive feature of the present model lies in designing the evolution equation of the surface variable. On a smaller length scale (in a  $10^{-7} - 10^{-6}$  cm range), we conjecture a dynamic pattern of surface phases, consisting of islands of a minority phase immersed in a continuous majority phase. Unlike the phenomenological model by Krischer, Eiswirth, and Ertl [9], we describe the surface state using a ‘‘microvariable’’  $u$  that can relax to two alternate states standing for the surface phases. The dynamics of the microvariable is described by a nonlinear diffusion equation with a cubic nonlinearity:

$$\gamma^{-1} u_t = \delta^2 \nabla^2 u + (1 - u^2)u - \alpha v, \quad (2)$$

where  $\delta \ll 1$  is the ratio of the microscopic and macroscopic scales, which is proportional in the physical model to the square root of the ratio of the surface diffusivities of Pt and CO (adsorbate). Since Pt diffusivity is small, the borders between the surface phases can be assumed to be almost atomically sharp.

The local value of long-range variable  $v$  introduces a bias in favor of one of the surface states. If the coupling parameter  $\alpha$  is positive, the lower state advances when the macrovariable  $v$  (modeling CO coverage) is positive. The two phases coexist at  $\alpha|v| < b = 2/\sqrt{27}$ . The speed of the motion (neglecting the curvature effect) is

$$c = \sqrt{6} \delta \gamma \sin\left[\frac{1}{3} \arcsin\left(\frac{1}{2} \sqrt{27} \alpha v\right)\right] \equiv \delta \gamma \psi(\alpha v). \quad (3)$$

The dynamics of the surface phases described by this model can be made similar to the dynamics of the surface variable in the phenomenological model of Krischer, Eiswirth, and Ertl [9]. The two values of the CO coverage where the definition of the phenomenological function is changed should correspond to the limits  $v = \pm b/\alpha$  of the range of  $v$  where the two surface states coexist.

The macrovariable  $v$  in turn is affected by the relative abundance of surface phases, described by the coarse-grained variable  $\eta$ . A general relation between  $\eta$  and  $u$  can be defined as

$$\eta(x) = \hat{\beta} \left( \int g(x, x') u(x') dx' - \hat{s} \right), \quad (4)$$

where  $g(x, x')$  is a coarse-graining kernel with a characteristic range of  $O(1)$  in the chosen dimensionless units and  $\hat{\beta}, \hat{s}$  are constants. Assuming sharp interphase borders,  $\eta$  can be directly related to the surface-averaged area covered by the lower surface state  $u < 0$ :

$$\eta(x) = \beta \left( \int g(x, x') H(x') dx' - s \right), \quad (5)$$

where  $H(x)$  is 1 if the point  $x$  is within a domain occupied by the lower state, and 0 otherwise, and  $\beta, s$  are modified constants.

## III. GLOBAL OSCILLATIONS

The simplest solution of the coarse-grained equations is obtained under conditions where the diffusional range of the macrovariable  $v$  encompasses the entire surface so that it plays the role of a global variable obeying Eq. (1) integrated over the entire surface:

$$v_t = (1 - v^2)v - \eta. \quad (6)$$

Then the integrals in Eqs. (4),(5) can be evaluated over the entire surface as well, and the coarse-graining kernel  $g(x, x')$  set to unity. If we assume that the lower surface state is a minority phase, and exists in the form of circular islands (sufficiently widely separated, so that their interaction can be neglected), Eq. (5) can be rewritten as

$$\eta = \beta \left( \int f(r) r^2 dr - s \right) = \beta (n \langle r^2 \rangle - s), \quad (7)$$

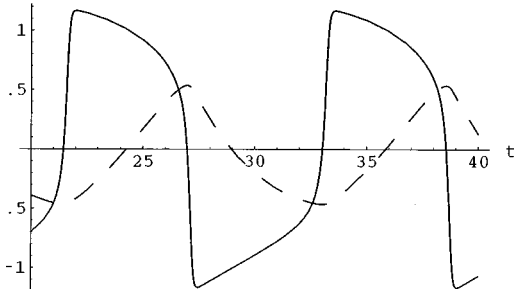


FIG. 1. A typical oscillation cycle at  $\gamma \ll 1$ ; dynamics of  $v$  and  $\eta$  are shown by solid and dashed curves, respectively.

where  $f(r)$  is the instantaneous number density of islands with the radius  $r$  and  $n$  is the total number density of islands. The parameter  $s$  can be interpreted as the surface fraction corresponding to the Maxwell construction of the two macrostates. This value serves in our model as a bias parameter. Assuming  $\beta > 0$ , negative values of  $v$  prevail at  $\eta > 0$ . The multistability range is  $|\eta| < b = 2/\sqrt{27}$ .

For the moment, we neglect the dependence of the boundary speed on the curvature (presuming that the islands are much larger than the diffusional range of the microvariable). Then the change of radii is governed by Eq. (3) which can be transformed by averaging to the evolution equation of  $\eta$ :

$$\frac{d\eta}{dt} = 2\beta n \delta \gamma \psi(\alpha v) \langle r \rangle(\eta). \quad (8)$$

For any fixed size distribution  $f(r)$ , the mean radius  $\langle r \rangle$  can be expressed through the mean squared radius  $\langle r^2 \rangle$ , and then expressed through  $\eta$  with the help of Eq. (7). As long as the dependence of the boundary dynamics on curvature is neglected, this is also possible for a dynamically evolving distribution. Indeed, the distribution is then shifted rigidly during the oscillation cycle so that  $f(r;t) = f(r + c(\eta)t)$  and, as a consequence, the dispersion  $\langle r^2 \rangle - \langle r \rangle^2$  remains invariant.

If all islands are of the same size,

$$\langle r \rangle = \sqrt{n^{-1}(s + \eta/\beta)} = \sqrt{s/n(1 + \eta/q)}, \quad (9)$$

where  $q = \beta s > b$ . The final form of Eq. (8) is

$$\frac{d\eta}{dt} = K \psi(\alpha v) \sqrt{1 + \eta/q}, \quad (10)$$

where  $K = 2\beta \delta \gamma \sqrt{sn}$ .

A typical picture of relaxation oscillations is obtained at  $\gamma \ll 1$ . Then the system evolves as follows. If, say, initially  $v > 0$ , the lower state advances and  $\eta$  increases. The macrovariable  $v$  continuously adjusts to a changing level of  $\eta$ ; it decreases but remains on the upper branch until  $\eta$  reaches the limiting value  $\eta = b$ . After this,  $v$  drops on a fast  $O(\gamma)$  time scale to the lower branch. The islands start to shrink, and  $v$  grows while  $\eta$  decreases up to the lower critical value  $\eta = -b$ , after which  $v$  jumps back to the upper branch (Fig. 1); both branches of the oscillation cycle are symmetric.

In the limiting case when the macrovariable  $v$  is slaved to  $\eta$ , it can be replaced in Eq. (8) by either the upper or lower root of the cubic  $(1 - v^2)v + \eta = 0$ , respectively  $v_{\pm}(\eta)$ . This

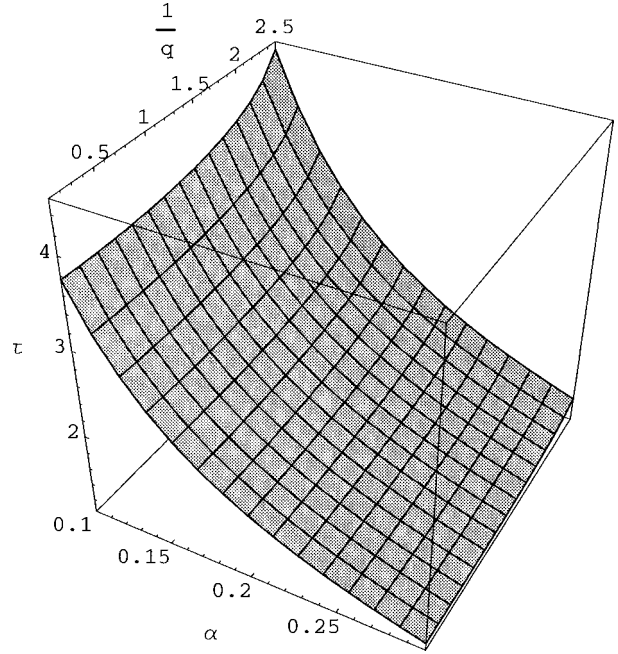


FIG. 2. The dependence of the rescaled period  $\tau$  on the rescaled bias parameter  $q$  and the coupling parameter  $\alpha$  at  $\gamma \ll 1$ .

leaves us with a single dynamic equation, and the rescaled half-period  $\tau = 2\beta \delta \sqrt{sn} T$  is computed as

$$\tau = \int_{-b}^b \frac{d\eta}{\sqrt{1 + \eta/q} \psi(\alpha v_{\pm}(\eta))}. \quad (11)$$

The dependence of  $\tau$  on the rescaled bias parameter  $q$  and the coupling parameter  $\alpha$  are shown in Fig. 2.

The above picture is modified if the changing levels of  $v$  remove the system from the multistability region of the microvariable or if islands shrink and disappear altogether while the system evolves along the branch  $v < 0$ . To preclude the first possibility, one has to require that the maximum possible value of  $v$  occurring during the above cycle,  $|v_{max}| = 2/\sqrt{3}$  remain within the multistability range. This restricts the value of the parameter  $\alpha < \frac{1}{3}$ . If all islands are of the same size, the minimum radius corresponding to  $\eta = -b$  in Eq. (7) is  $r_{min} = \sqrt{n^{-1}(s - b/\beta)}$ , which restricts the parameter  $\beta > b/s$ .

An arbitrary distribution can be treated in a similar way. For example, for a uniform distribution of island sizes in the range  $\langle r \rangle - \frac{1}{2}\Delta < r < \langle r \rangle + \frac{1}{2}\Delta$ , the required relation between the mean and mean squared radii is given by  $\langle r^2 \rangle = \langle r \rangle^2 - \frac{1}{12}\Delta^2$ , so that the radicant in Eq. (9) should be increased by  $\frac{1}{12}\Delta^2$ .

The lower tail of a distribution of island sizes may be eliminated during a single cycle, but, as long as the curvature effect can be neglected, the residual distribution will remain stationary (or, more precisely, will rigidly oscillate). The curvature effect should be felt, however, in the long run, causing a kind of Ostwald ripening under nonstationary conditions (see Sec. V).

#### IV. LOCALIZED OSCILLATIONS AND WAVES IN AN EXTENDED SYSTEM

In an extended system ( $L \gg 1$ ), Eq. (8) can still be retained as a dynamic equation of  $\eta$ , with local averaging understood as in Eq. (5). At  $\gamma \ll 1$ , the system relaxes (starting from random initial conditions) to a pattern containing domains with prevailing alternative states of the macrovariable. The overall character of macroscopic dynamics depends on the value of the dimensionless combination  $K$ . The ideal form of a propagating plane wave at  $K \ll 1$  is computed in a standard way by applying a relation analogous to Eq. (3) to determine the speed of the macroscopic front

$$C = \sqrt{6} \sin\left[\frac{1}{3} \arcsin\left(\frac{1}{2} \sqrt{27} \eta\right)\right] \equiv \psi(\eta), \quad (12)$$

and then integrating Eq. (10) in the frame moving with this speed. The resulting half period in space is just  $\tau C$ , where  $\tau$  is the half-period of the global oscillation cycle defined by Eq. (11).

At moderately small values of  $K$ , a simulation run starting from random initial conditions leads, following an initial relaxation period, to domain oscillations that may be also characterized as a highly unharmonic standing wave pattern. A typical relaxation oscillation cycle is shown in Fig. 3. In the first snapshot, the upper state (shown in the light end of the grayscale) is a minority phase forming bean-shaped macroislands. These islands grow through front propagation, while macroislands of the alternative lower state (shown in dark grays) nucleate within, i.e., at locations that have been occupied by the upper state for a long period of time.

The propagation does not, however, proceed all the way to coalescence of upper-state islands, but is assisted by a bulk transition within the lower majority state. The transition moment is captured in Fig. 3(c). Following the transition, the upper state becomes the majority state, leaving recently nucleated islands of the lower state. As a result, the last snapshot in the series looks very much like a negative of the original one. This completes the half period of the oscillation cycle, whereafter the story repeats with the islands of the alternate state but the size of the islands slightly increases. At this stage, the overall picture combines features of front propagation and coherent oscillations but the pattern is still transitory. The region of coherent oscillations gradually shrinks, and the final state achieved in the long run is a disordered spiral pattern (Fig. 4).

#### V. RIPENING OF SURFACE PHASE DISTRIBUTION

The size distribution of islands of the minority phases evolves at long times due to a weak dependence of the velocity on curvature:

$$c = \delta\gamma[\psi(\alpha v) - \kappa\delta]. \quad (13)$$

For circular islands,  $\kappa = r^{-1}$ , and the dynamic equation for radii is

$$\frac{dr}{dt} \equiv c(v, r) = \delta\gamma \left[ \psi(\alpha v) - \frac{\delta}{r} \right]. \quad (14)$$

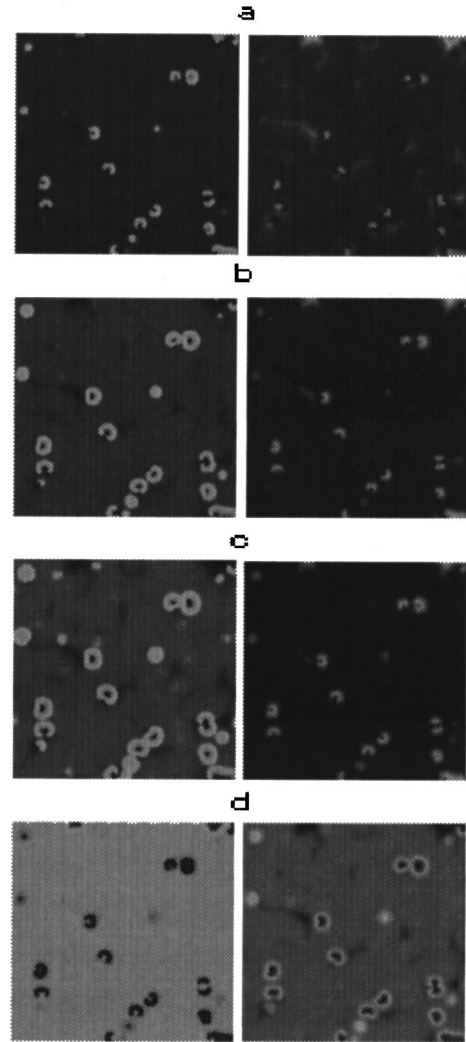


FIG. 3. A typical transitory oscillation cycle in an extended system ( $q=0.56$ ,  $K=0.05$ ,  $\alpha=0.3$ ). Snapshots taken at (a)  $t=118$ , (b)  $t=127$ , (c)  $t=131$  (transition moment), (d)  $t=151$ . Levels of the macrovariables  $v$  (left) and  $\eta$  (right) are shown in gray scale.

The radius distribution necessary for evaluation of the surface area occupied by the minority phase in Eq. (7) obeys the first-order partial differential equation (PDE)

$$\frac{\partial f}{\partial t} + \frac{\partial(fc(v, r))}{\partial r} = 0, \quad (15)$$

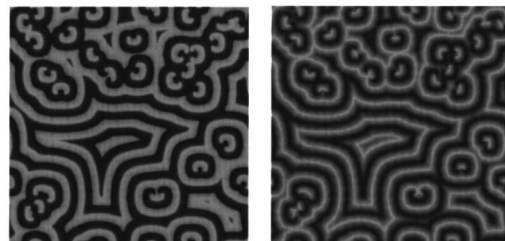


FIG. 4. A disordered spiral pattern in an extended system ( $q=0.56$ ,  $K=0.05$ ,  $\alpha=0.3$ ,  $t=2000$ ). Levels of the macrovariables  $v$  (left) and  $\eta$  (right) are shown in gray scale.

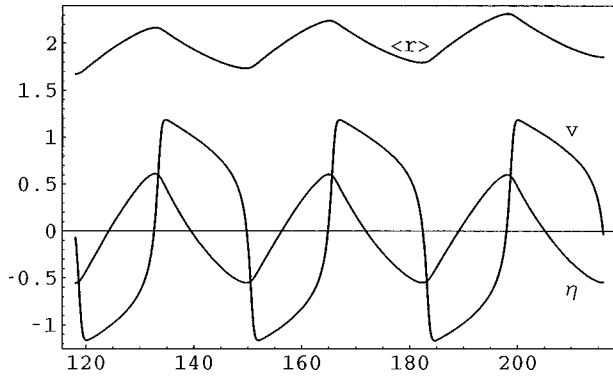


FIG. 5. Short-scale dynamics of the global variable  $v$ , the coverage fraction  $\eta$ , and the mean radius ( $\delta=0.02$ ,  $s=2.7$ ,  $\beta=0.9$ ,  $\alpha=0.2$ ,  $\gamma=4.0$ ).

which has to be solved together with Eq. (6) where  $\eta$  is defined by Eq. (7). Since the velocity  $c(v,r)$  changes sign during the oscillation cycle, Eq. (15) is ill-suited to a common finite difference scheme of numerical integration but is readily solved by the method of characteristics. The characteristics are defined by Eq. (14); since  $c(v,r)$  is a monotonic function of  $r$ , shocks are never formed, and the distribution is well behaved. The ripening process should generally lead to slow elimination of smaller islands and growth of the average island size.

Figure 5 shows the dynamics of the global variable  $v$ , the coverage fraction  $\eta$ , and the mean radius over the length of several periods. The form and period of oscillations changes slowly, in parallel with slow evolution of the island size distribution. The long-time dynamics of statistical characteristics starting from a Gaussian distribution is shown in Fig. 6. To eliminate short-scale dynamics, all values are computed here at the lowest point of each oscillation cycle. Dispersion gradually increases, while the skewness becomes negative. Elimination of smaller islands becomes substantial after the lower tail of the distribution has reached the lower cutoff radius. Following this, the island number density decreases, the growth of the mean radius accelerates, and the trend of the evolution of the skewness reverses, reflecting preferential growth of larger islands. The total area occupied by the islands at the lowest point of each oscillation cycle (as at any other comparable phase of the cycle) remains constant to a high degree of accuracy.

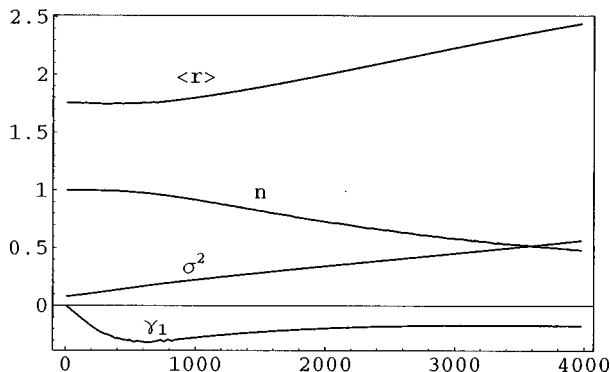


FIG. 6. Long-scale dynamics of the number of islands  $n$ , mean radius  $\langle r \rangle$ , dispersion  $\sigma^2$ , and skewness  $\gamma_1$  of the island size distribution ( $\delta=0.02$ ,  $s=2.7$ ,  $\beta=0.9$ ,  $\alpha=0.2$ ,  $\gamma=4.0$ ).

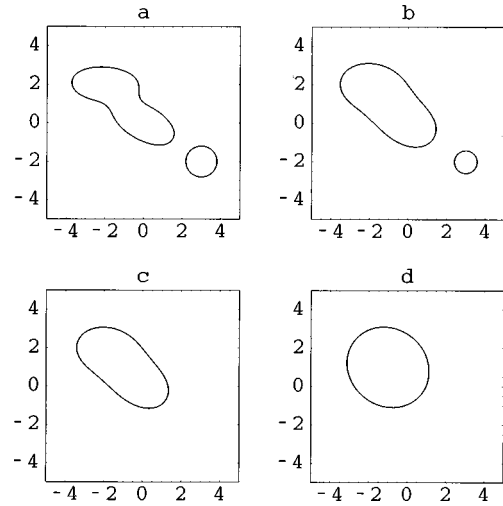


FIG. 7. Snapshots of the ripening sequence taken at (a)  $t=2$ , (b)  $t=10$ , (c)  $t=12$ , and (d)  $t=66$  ( $\delta=0.02$ ,  $s=13.3$ ,  $\beta=1.42$ ,  $\alpha=0.2$ ,  $\gamma=0.2$ ).

The growth process may be arrested by the instability of large islands. Saturation of growth can be accounted for phenomenologically by introducing a dependence of the growth rate on curvature that has a maximum at a certain point [19].

### VI. BOUNDARY DYNAMICS

The presumption of a circular shape is well justified only when the interaction between islands is negligible. At higher densities of the minority phase, or, moreover, under conditions when the phases are interspersed and neither forms a connected continuum, the boundary dynamics is governed locally by Eq. (13) but the radius distribution is not well defined.

We have carried out detailed modeling of the ripening process with the help of a Lagrangian algorithm based on the local equation of boundary motion. Each island is represented by its boundary which in turn is approximated as a polygon, i.e., a directed array of the points in a plane, which propagates according to Eq. (13) with the velocity dependent on the instantaneous value of  $v$  and the local curvature approximated by finite differences. The long-scale variable  $v$  is

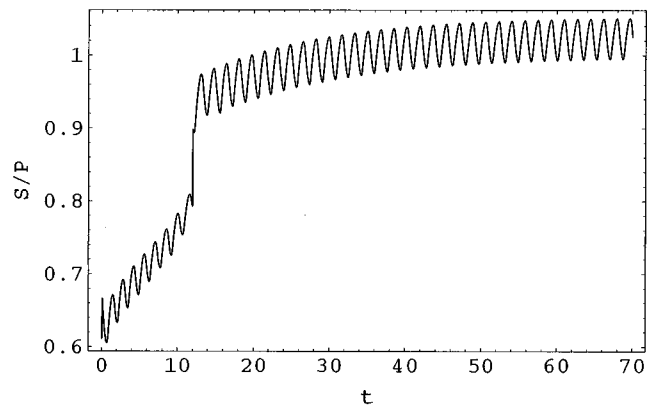


FIG. 8. Dynamics of average radius (defined as ratio of total ratio  $S$  of islands to their total perimeter  $P$ ) corresponding to the sequence shown in Fig. 7. A sharp jump at  $t \sim 12$  corresponds to elimination of the smaller island.

treated also in these computations as a global variable, and its dynamics determined by Eq. (6), where  $\eta$  is expressed through the total instantaneous area of the islands. The computation algorithm includes updating the boundary, checking for intersections, computation of the area, and updating of  $v$ .

A typical ripening sequence obtained by numerical simulation is shown in Fig. 7. As expected, the ripening process leads to elimination of smaller islands, while the surviving islands approach a circular shape. The average radius, defined as the ratio of the perimeter to the area occupied by the minority phase, exhibits steady growth on the background of oscillations as seen in Fig. 8.

The ripening can be suppressed on a rough surface. Self-induced roughening may be caused by surface modification taking place at locations traversed by the transition front between the alternate surface states. The surface modification may also compensate the ripening process by gradually lowering the upper limit of island growth during an oscillation cycle. The effect of stabilization of surface phase distribution due to reactive roughening will be described in a forthcoming paper.

## VII. CONCLUSION

The two-tier model described above combines features found in the standard FitzHugh-Nagumo model at different ratios of characteristic relaxation times and diffusivities of the species involved. On the macroscopic level,  $v$  is a fast activator, while  $\eta$  plays at  $\gamma \ll 1$  the role of a nondiffusive slow inhibitor. At the same time, on the microscopic level,  $u$  is a slow short-range activator while  $v$  is a fast long-range inhibitor. The two levels are related by the averaging procedure defining the evolution equation of  $\eta$ . The physical origin of the averaging is in sampling of large surface areas by the diffusive macrovariable.

The distribution of surface phases ripens at long times due to preferential growth of larger islands. The ripening process may be arrested by surface inhomogeneities, either nascent or developing dynamically in the course of the process.

## ACKNOWLEDGMENT

This research was supported by the Ministry of Science and Arts of Niedersachsen.

- 
- [1] M. Eisinger and G. Ertl, in *Chemical Waves and Patterns*, edited by R. Kapral and K. Showalter, (Kluwer, Dordrecht, 1994).
  - [2] R. Imbihl and G. Ertl, *Chem. Rev.* **95**, 697 (1995).
  - [3] S. Jakubith, H.-H. Rotermund, W. Engel, A. von Oertzen, and G. Ertl, *Phys. Rev. Lett.* **65**, 3013 (1990).
  - [4] G. Ertl, *Science* **254**, 1756 (1991).
  - [5] K. C. Rose, D. Battogtokh, A. Mikhailov, R. Imbihl, W. Engel, and A. M. Bradshaw, *Phys. Rev. Lett.* **76**, 3582 (1996).
  - [6] K. C. Rose, B. Berton, R. Imbihl, W. Engel, and A. M. Bradshaw (unpublished).
  - [7] R. Imbihl, M. P. Cox, G. Ertl, H. Müller, and W. Brenig, *J. Chem. Phys.* **83**, 1578 (1985).
  - [8] M. Eisinger, P. Möller, K. Wetzl, R. Imbihl, and G. Ertl, *J. Chem. Phys.* **90**, 510 (1989).
  - [9] K. Krischer, M. Eisinger, and G. Ertl, *J. Chem. Phys.* **96**, 9161 (1992).
  - [10] M. Bär, M. Hildebrand, M. Eisinger, M. Falcke, H. Engel, and M. Neufeld, *Chaos* **4**, 499 (1994).
  - [11] M. Falcke, M. Bär, H. Engel, and M. Eisinger, *J. Chem. Phys.* **97**, 4555 (1992).
  - [12] M. Bär, S. Nettesheim, H.-H. Rotermund, M. Eisinger, and G. Ertl, *Phys. Rev. Lett.* **69**, 945 (1992).
  - [13] H. Levine and X. Zou, *Phys. Rev. Lett.* **69**, 204 (1992); *Phys. Rev. E* **48**, 50 (1993).
  - [14] M. Falcke and H. Engel, *Phys. Rev. E* **50**, 1353 (1994); *J. Chem. Phys.* **101**, 6255 (1994).
  - [15] S. Ladas, R. Imbihl, and G. Ertl, *Surf. Sci.* **197**, 153 (1988); **198**, 42 (1988).
  - [16] R. Imbihl, A. E. Reynolds, and D. Kaletta, *Phys. Rev. Lett.* **67**, 275 (1991).
  - [17] R. Imbihl, *Mod. Phys. Lett. B* **6**, 493 (1992).
  - [18] T. Gritsch, D. Coulman, R. J. Behm, and G. Ertl, *Phys. Rev. Lett.* **63**, 1086 (1989).
  - [19] A. Hagberg and E. Meron, *Phys. Rev. Lett.* **72**, 2494 (1994).